A low-cost and easy-to-use phantom for cone-beam geometry calibration of a tomographic X-ray system

V. Nguyen[1], J. De Beenhouwer[1], J.G. Sanctorum[2], S. Van Wassenbergh[3], P. Aerts[3], C. Van Ginneken[4], J. J. J. Dirckx[2], J. Sijbers[1]

[1]imec - Vision Lab, Department of Physics, University of Antwerp, Universiteitsplein 1, Antwerp 2610, Belgium
[2]Biophysics and BioMedical Physics (BIMEF) Lab, University of Antwerp, Belgium
[3]Functional Morphology Lab, University of Antwerp, Belgium
[4]Applied Veterinary Morphology Lab, University of Antwerp, Belgium
e-mail:{van.nguyen, jan.debeenhouwer, joaquim.sanctorum, sam.vanwassenbergh, peter.aerts, chris.vanginneken, joris.dirckx, jan.sijbers}@uantwerpen.be

Abstract
Knowledge of the acquisition geometry is key for tomographic reconstruction. Before image reconstruction algorithms can be applied to compute a 3D image from a set of 2D projections, calibration must be carried out to correct geometrical inaccuracies. The main source of geometric misalignment can be attributed to possible mechanical instability and slight offsets in rotation and translation of the source, detector and/or the sample stage themselves from the measured parameters. Although, many studies have been dealing with the calibration problems for a specific X-ray CT system, most of those methods require specifically-designed and/or expensive phantoms. In this work, we introduce a low-cost, easy-to-use and readily available phantom, built from LEGO bricks that serves as a structure to hold small, 'metal' beads for geometric calibration of a tomographic X-ray system.

Keywords: cone-beam geometry, calibration, LEGO phantom

1 Introduction

A large number of studies have been dealing with calibration of X-ray acquisition systems, as knowing the geometry parameters is crucial to achieve high quality tomographic reconstructions. In general, calibration techniques can be divided into two main categories which include the techniques using a calibration phantom [2–4, 9, 11] and self-calibration methods [6, 12] that exploit the acquired radiographs of the target objects for calculating the geometry parameters of their acquisition systems.
Most X-ray CT calibration methods that rely on a phantom, require specifically-designed and/or expensive phantoms with marker features placed at accurately-known positions in the bearing structures and measured precisely using Coordinate Measuring Machines (CMM) which are often not available in most X-ray imaging laboratories [3, 4, 9]. Among them, Liu et al. [9] introduced a phantom that carried 12-sphere Zirconia markers placed on a triple helix glass structure. Furthermore, the phantom was built from made-to-order components, and hence not always easily available. Another well-designed phantom was presented by Cho et al. and Chetley et al. [3, 4] and featured two circular rings of regular placed steel balls carried on an acrylic cylinder. Both the diameters of the supporting cylinder and the steel balls were measured in advance. However, it is not trivial to place the steel balls at equidistant positions on the supporting cylinder without using specific devices to navigate the placements to the exact desired positions.
Several methods investigated radiographs as reference data for calibration as presented in [6, 12], but only calculated a limited number of parameters. Parkinson et al. [12] proposed a specifically designed algorithm to a certain type of datasets which exploited geometric characteristic of target object's projections, hence it is difficult to implement to the other acquisition systems. Kingston et al. [6] estimated geometrical misalignment by iteratively refining the sharpness of reconstructed images. In this method, the authors only considered four misalignment parameters, while requiring reconstructed CT images for calculating the sharpness fitness function, which was computationally expensive when applying to a 3D CT system. Our purpose is to present a reliable calibration technique, using a low-cost phantom, that can be easily and readily implemented for various X-ray systems.
From computational point-of-view, there are two main categories including analytic calculation and least squares optimization methods. Analytic methods such as the one introduced by Parkinson et al. [12] could be used to estimate rigid transformations on the 2D projections which are the weak representations of the 3D geometrical misalignment in the practical situations since the out-of-plane transformations were not taken into account. Furthermore, since the method investigated the edges of the cylindrical capillary tube, which was used to hold the target object, as the reference margins to calculate the orientation angle of the rotation axis, the algorithm is difficult to apply to other X-ray CT systems.
Another analytic method was introduced by Azevedo et al. [2] where only the rotation axis center was calculated by fitting a three-parameter sinusoid to the marker projection center-of-masses extracted from the radiographs. The problem was simplified to matrix form so that only matrix operators were applied to calculate the shifts of the rotation axis with respect to the detector center. In another study, F. Noo et al. [11] calculated seven parameters directly from fitted ellipses onto the projection trajectories

of two markers' centers. Generally, analytic methods require careful analysis of the geometry setting of the system, which results in increasing complexity as more parameters are considered when propagating to the other systems.
The least squares optimization approaches such as described by Gullberg et al. [5], have the advantage that they can easily be applied to other systems, without reformulation of the analytic formulas. Therefore, we will present a calibration algorithm based on least squares optimization to estimate the set of geometrical parameters to keep our solution as simple as possible such that it can be easily applied to other X-ray systems.
As calibration phantoms are generally expensive or complex to construct, there have been attempts to build phantoms from affordable LEGO bricks. LEGO elements were first introduced in an approach to construct a mounting structure of an optical system exploiting their characteristics such as small geometrical tolerances that are less than 20μm off from the designed shape and size [13]. Moreover, the variations in shapes and sizes of the LEGO bricks make them excellent components to build a calibration phantom which can adapt to different systems. In addition, Levine et al. [7] used LEGO elements to build a calibration phantom for a CT system where the authors designed a phantom consisting of two LEGO spacers holding three spheres as the calibration markers. The position of the spheres were measured by a CMM and the phantom was used to detect the systematic errors of a medical X-ray scanning system. Therefore, by using LEGO bricks to build a supporting structure, we can achieve significant accuracy in locating the position of the markers on the supporting structure as well as exploit their availability to have a simple but effective solution for calibrating an X-ray system.
In this paper, we introduce a calibration method using a LEGO phantom with metal beads placed at different positions underneath the bearing bricks. By using LEGO bricks and metal beads, our phantom easily adapts to various X-ray CT systems. Additionally, the estimation process is conducted using least squares optimization which allows our algorithm to be easily applied to other CT systems with different geometry parameters. In the rest of this paper, section 2 will present our proposed methodology to build a calibration phantom using LEGO bricks and metal beads along with the process to estimate the geometrical misalignments using a fast least squares optimization. Section 3 will discuss in detail the experiments on the simulation datasets to validate the feasibility of our proposed method as well as the experiments and results on a real LEGO phantom. Finally, further discussion and conclusion will be expressed in section 4.

2 Methodology

Acquisition system Figure 1 shows the dual-energy X-ray system that is used for the experimental measurements: The 3-Dimensional DYnamic MOrphology using X-rays (3D^{2}YMOX) system, dedicated to morphological research [1]. This system is highly modular such that geometrical calibration is required after each new setup. The system consists of two orthogonal X-ray source-detector pairs.

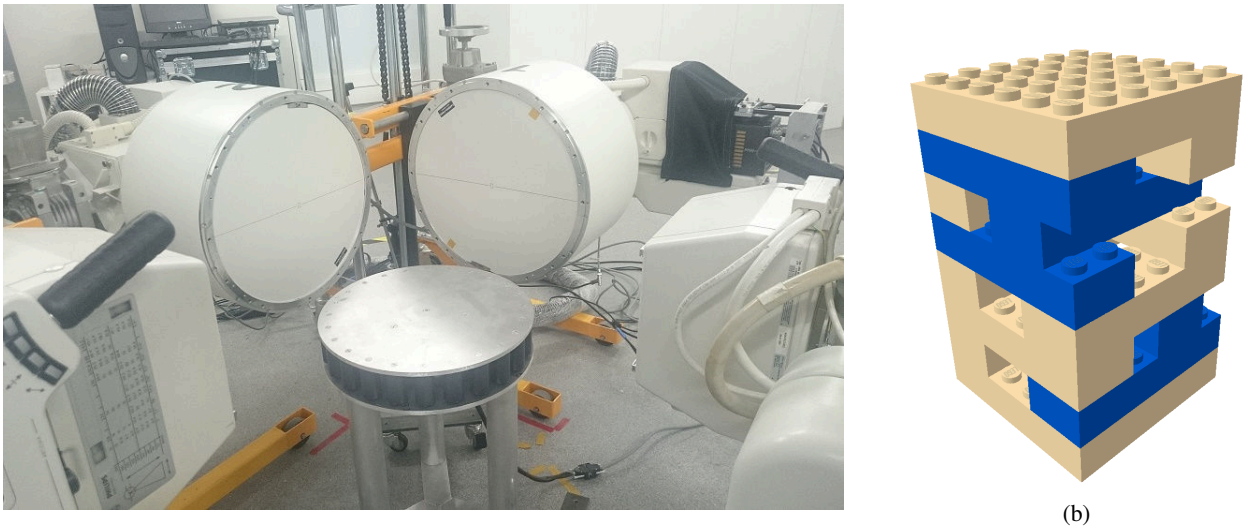

(a) (b)

Figure 1: 3D^{2}YMOX system (a) and an example of a LEGO phantom (b).

Each component in the 3D^{2}YMOX system has six degrees-of-freedom representing its position and orientation in 3D world. Without using an accurate manipulation system, it is difficult to align the source, detector and rotation stage properly or to measure the geometrical parameters accurately. Therefore, it is essential to carry out a calibration process so that the system geometry can be estimated as accurately as possible.

2.1 LEGO phantom design strategy

Our phantom's supporting structure was built using as few LEGO bricks as possible so as to avoid high attenuation of the X-rays and enhance the contrast between the projections of the LEGO module and the metal beads in order to easily extract the metal bead centers from the projection data. The metal beads were placed underneath the hollow tubes of the LEGO bricks at different positions in the phantom such that no two beads are within the same plane orthogonal to the rotation axis (marked as the blue bricks in figure 1b). The metal beads were placed such that their projection trajectories covered as much of the detector's field-of-view as possible. Depending on the size of the field-of-view of the target system, the size of the holding structure and the number of metal beads can easily be adjusted accordingly. The dimensions of the LEGO bricks and the positions of metal beads were measured by an electronic ruler with 10 μm accuracy.

2.2 Geometry parameterization

Figure 2 shows a general cone-beam geometry (in black) where the rotation axis is aligned to the source and the detector vertical center axis. In this aligned geometry, the position of the rotation axis is considered as the 'isocenter', the source-detector distance (SDD) and the rotation axis-detector distance (SOD) refer to the shortest paths from the source to the detector and from the source to the isocenter, respectively. The cone-beam geometry in blue, illustrates a misalignment in the form of a rotation axis displacement from the orthogonal plane containing the source and detector's vertical axis. To handle this geometrical misalignment, the geometry was parameterized with 10 degrees-of-freedoms including object translations (offsets of the object center-of-mass against the isocenter with respect to three axes (Δx^o, Δy^o, Δz^o), object orientations (η^o, θ^o, ϕ^o), rotation axis translations along horizontal axes (Δx^w, Δz^w) and rotation axis orientations (η^w, ϕ^w).

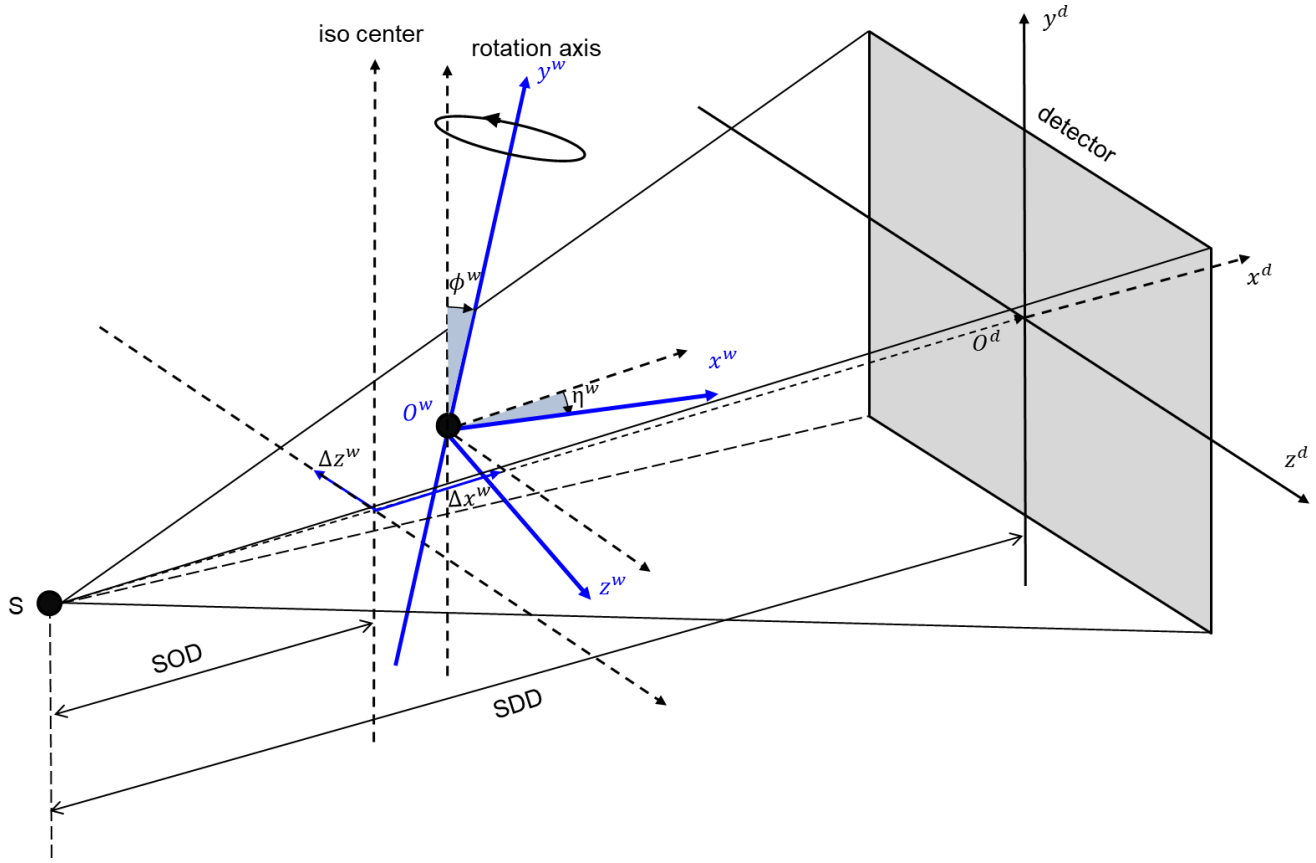

Figure 2: Visualization of a cone-beam geometry.

Data preprocessing The projection coordinates of the metal bead centers are used as input for the geometry estimation algorithm. However, the acquired radiographs from the 3D^{2}YMOX system suffered from geometrical distortion of the image intensifier and non-uniform detector pixel response. Therefore, acquired radiographs were preprocessed to eliminate the pincushion distortion effect of the image intensifier. Next, flatfield and log correction was applied to remove the variations in the pixel-to-pixel intensity of the detector. The corrected projection data could then be used for a template matching approach [8] in which the Normalized Cross Correlation (NCC) is calculated using a template in the frequency domain. The template was generated as a simulated forward projection of a single metal bead in the cone-beam geometry using the initial measurements acquired with a laser meter. The simulation was conducted using the CAD (Computer-aided design) projector framework [10]. This framework allowed us

to generate the X-ray forward projections of a certain CAD model with a simulated cone-beam geometry at a certain energy spectrum. The metal bead centers were calculated as the center-of-masses of 3x3 windows on the NCC images where the NCC values were local maxima. The projection trajectory of each metal bead center was extracted by minimizing the coordinate distance between neighboring projections.

Projection coordinate synthesizing The synthesized projection coordinates (y^s, z^s) of the metal bead centers were generated by applying a conventional ray-tracing technique in which the intersections of the lines connecting the source point, the metal bead centers (x^o, y^o, z^o) and the detector at certain projection angles were calculated. At each angle, the geometry was transformed accordingly with respect to the geometrical parameters using the ASTRA Toolbox vector geometry [14]. Therefore the projection trajectories of the metal bead centers reflected the desired geometry misalignment.

Geometry estimation Similar to [5], geometrical parameters β were estimated by iteratively minimizing total Euclidean norms χ between synthesized (y_i^s, z_i^s) and measured (y_i^m, z_i^m) projection coordinates over all the projection angles p_i (i = [1, N]):

$$argmin_\beta\{\chi|\chi = \sum_{i=1}^{N}(y_i^s(\beta) - {y_i}^m)^2 + (z_i^s(\beta) - {z_i}^m)^2\} \tag{1}$$

where $\beta = \{\Delta x^o, \Delta y^o, \Delta z^o, \eta^o, \theta^o, \phi^o, \Delta x^w, \Delta z^w, \eta^w, \phi^w\}$.

3 Experiments and results

Our methodology was validated using simulated and measured datasets. The simulated datasets contained 720 equiangular projections over 360 degrees for which the cone-beam geometry was manipulated by 10 parameters to simulate 10 'unknown' components of geometrical misalignment. To generate this dataset, we first constructed a mesh representation of our calibration phantom. Next, the ASTRA CAD projector [10] was used to simulate the forward projections in the transformed geometry. Afterwards, noise was added with varying variances [0, 0.8] to the projection data that maximum intensity level is one. The measured datasets contained 751 projections equiangularly distributed over 360 degrees. All the simulated and measured datasets were preprocessed as described in section 2 to extract the trajectories of the markers in the projection space. In figure 3, we show the samples of a simulated radiograph without noise (fig. 3a), with a zero-mean Gaussian noise standard deviation $\sigma = 0.8$ (fig 3b), and a real radiograph acquired from the 3D^{2}YMOX (fig. 3c)

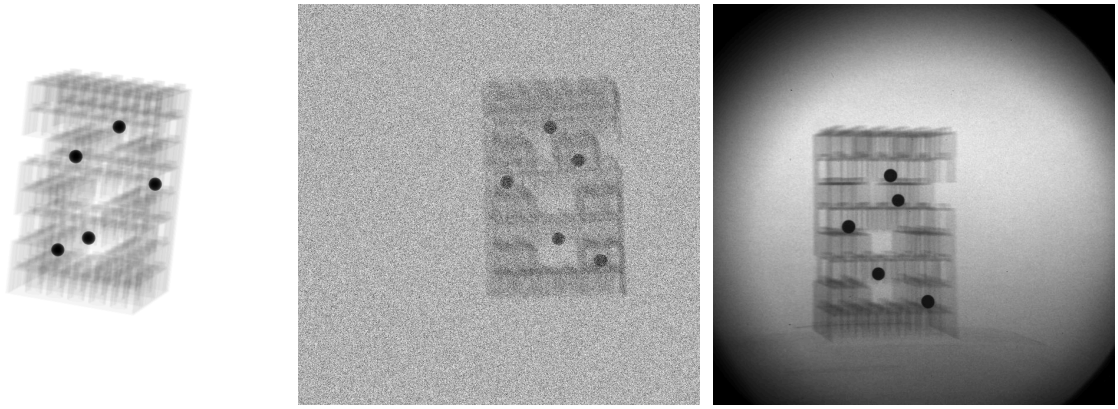

(a) (b) (c)

Figure 3: Samples of a noiseless radiograph (a), a noisy simulated radiograph (Gaussian noise $\sigma = 0.8$) (b), and a real radiograph acquired from the 3D^{2}YMOX system.

3.1 Experiments and results on simulated datasets

The experiment on the simulated data was used to evaluate the feasibility of the proposed calibration method. A first experiment was performed to evaluate the estimation of the geometry parameters in the presence of noise. At the start, all geometrical parameters were initialized to their initial values (i.e. zero offset from the acquisition parameters). To be able to demonstrate the experimental results clearly in the plots, we separated the geometrical parameters into two groups including orientation (η^o, θ^o, ϕ^o, η^w, ϕ^w) and translation (Δx^o, Δy^o, Δz^o, Δx^w, Δz^w) parameters. As shown in figures 4 and 5, the errors between estimated geometrical parameters and the ground-truths are steady and notably small (less than 1.2 mrad for angular parameters and 0.05 mm for translation parameters except the rotation axis translation Δx^w) compared to the original modifications. Moreover, as the noise levels increase significantly (zero-mean Gaussian noises with standard deviation σ varies in the range [0, 0.8]), the errors are not propagated correspondingly showing that our calibration process is robust to the influence of noise.

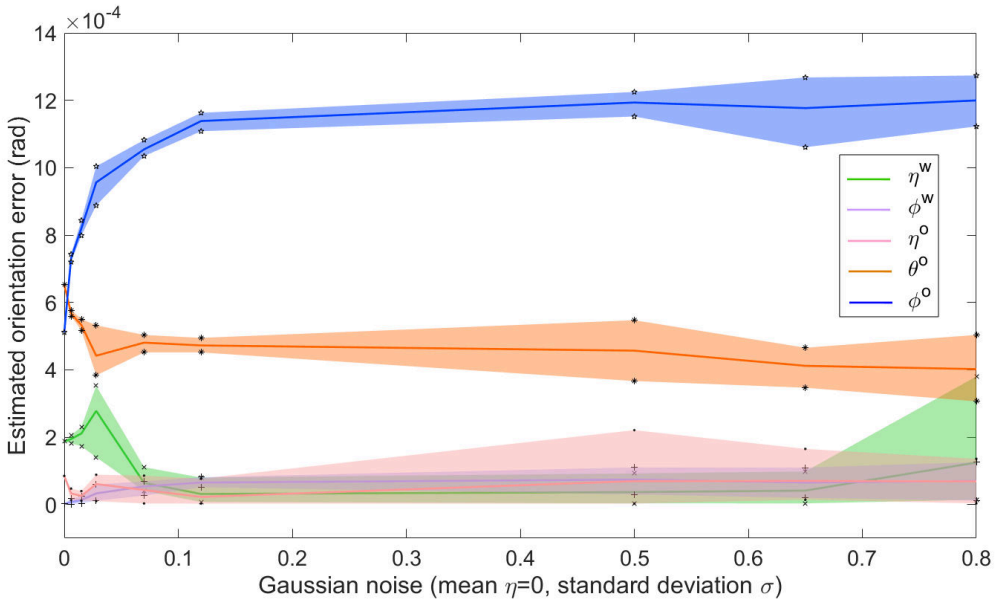

Figure 4: Estimation errors of the orientation parameters using the datasets simulated with different noise levels. The errors are below 1.2 mrad which will not introduce motion artefacts into tomographic reconstruction.

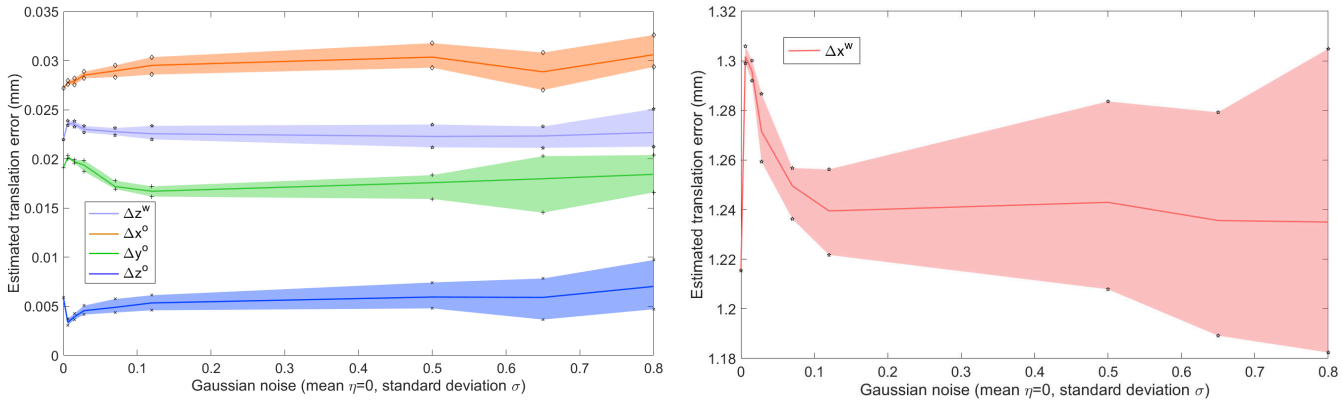

(a) (b)

Figure 5: Estimation errors of the translation parameters using the simulated datasets with different noise levels. The errors are below 0.05 mm except the rotation axis horizontal translation Δx^w deviated approximately one mm from the ground-truth.

In a second experiment, we examined the calibration performance as a function of the number of projections. The projection angles were shifted and the projections were chosen by evenly dividing the projection space into corresponding desired number of angles. As shown in figures 6 and 7, when decreasing the number of taken projections to as few as 10 projections, the errors do not ascend significantly.

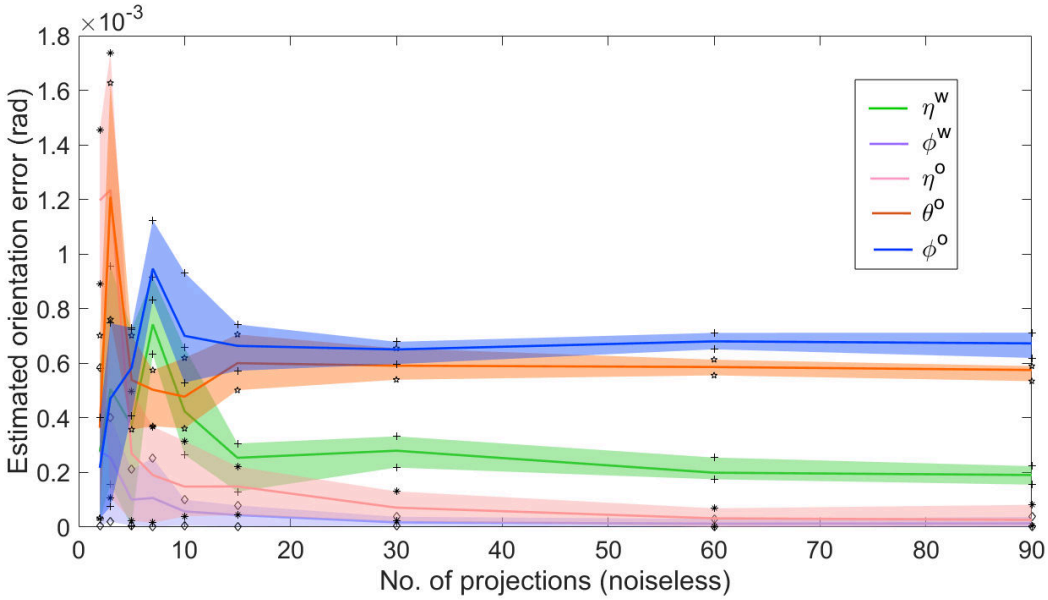

Figure 6: Estimation errors of the orientation parameters in the experiments using different number of projections. The errors are less than one mrad which will not introduce motion artifact into the reconstruction

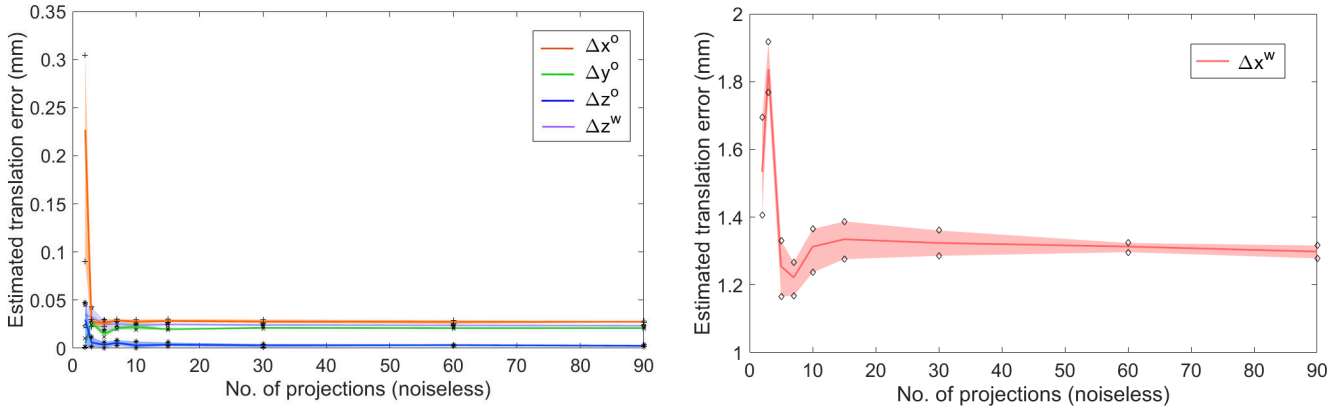

(a) (b)

Figure 7: Estimation errors of the translation parameters in the experiments using different number of projections.

In figures 5b and 7b, we observe the appearance of the outliers (1.3 mm) in the rotation axis translation parameter (Δx^w) which are notably larger than the medial errors (0.05mm). These can be attributed to the accumulated errors from the other parameters since geometrical parameters are highly correlated in nature. This hypothesis is substantiated in figure 8 where we show the coordinate distance between the trajectories generated using estimated parameters and the synthesized trajectories. The largest distance is approximate to two pixels. On average, the differences are scattered in the area of 0.5 pixel (presented as the white-black dots on the plot). Moreover, such moderate error indicates the estimated parameters are able to accurately describe the geometry misalignment introduced in the original simulation. Furthermore, as explicitly shown in the figure, our algorithm can also achieve sub-pixel accuracy in calibration. This close match is a strong consolidation of the feasibility of our proposed calibration process which will be able to apply to estimate geometry parameters of the real system.

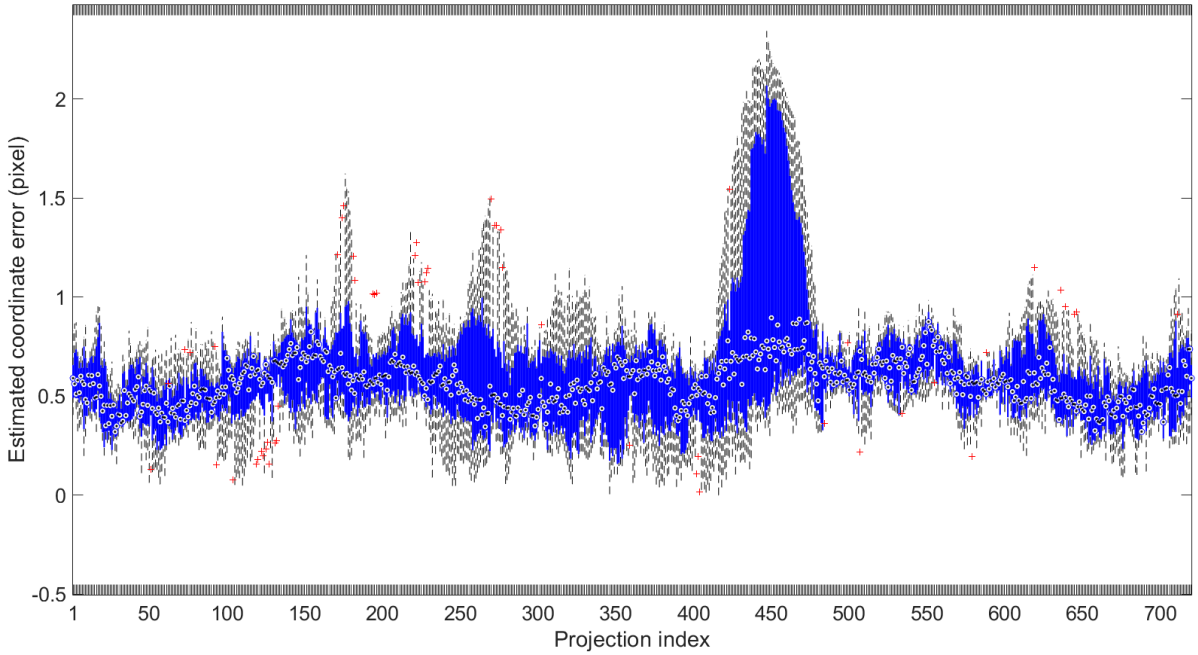

Figure 8: Average coordinate distances between estimated and simulated trajectories of the metal bead centers in the projection space (simulated dataset without noise).

Experiment on different number of metal beads This experiment was used to evaluate a suitable number of the metal beads to build a calibration phantom yet it also depends on the size of the target system. Theoretically, the more number of the metal beads was used, the better calibration results we would achieve. However, as to avoid overlapping of the metal bead projections on the detector, defining strategic number of metal beads is crucial in designing calibration phantom. Initially, five metal beads were used for the alignment, this number was then adjusted by one decrement in each try. Lastly, there was only one metal bead left to calibrate the system. The results were summarized in figures 9a and 9b. The estimation errors are significantly large when the number of metal beads is less than three. As three or more metal beads were use, the estimation error drastically decrease indicating that three or more metal beads are capable to calibrate the current system.

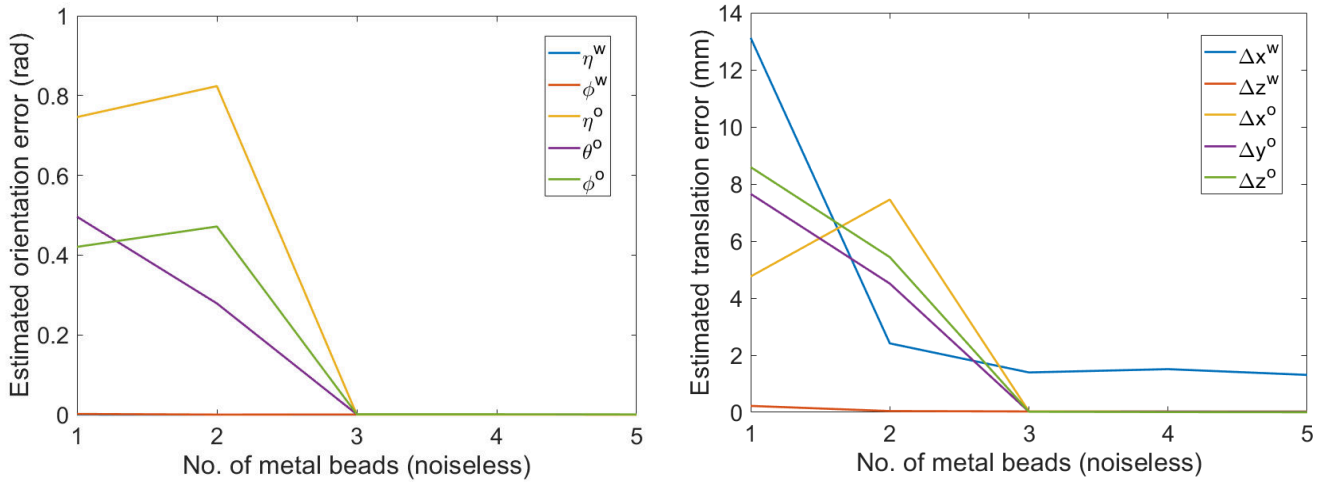

(a) (b)

Figure 9: Estimation errors of the orientation (a) and translation (b) parameters in the experiments using different number of metal beads.

3.2 Experiments and results on real dataset

Next, a real LEGO phantom was used to calibrate the geometrical setting of the 3D^{2}YMOX system. The calibration phantom radiographs were acquired using the 3D^{2}YMOX system where the source-detector and rotation axis-detector distances were empirically measured using a laser meter. Figure 10 illustrates the average projection coordinate distance over the projection

angles between estimated and measured trajectories. As shown in the figure, maximum difference is around six pixels. In general, the differences are distributed mostly in the range from two to four pixels (captured as the white-black dots on the figure).

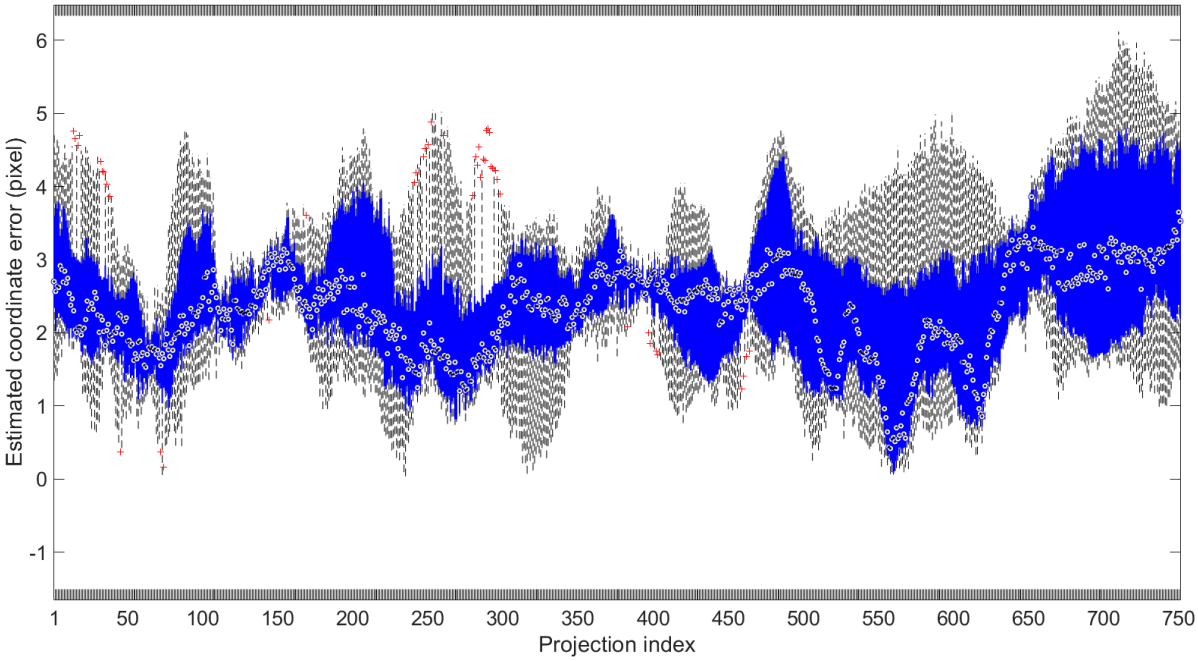

Figure 10: Average coordinate distances between estimated and measured trajectories of the metal bead centers in the projection space (calibration phantom bearing five metal beads).

4 Discussion

The results on simulated and real datasets demonstrated the robustness and stability of our proposed technique to build and use a LEGO phantom for calibrating arbitrary X-ray systems targeted to a low-cost and easy-to-use solution. By exploring LEGO bricks to build the supporting structure, we have high flexibility to adapt the shape and size of the phantom to the desired dimensions. LEGO bricks are made from Acrylonitrile Butadiene Styrene (ABS) which is a polyme having low attenuation coefficient to X-ray energies spectrum usually used in common X-ray systems. Therefore, the supporting structure is almost transparent in the acquired radiographs which facilitates the estimation of the metal bead centers.

Moreover, the estimation algorithm did not use the intensity differences as the criteria for least squares optimization. Therefore noise was not propagated correspondingly to the estimation. The process to extract center coordinates of the metal beads relied on the calculation of the NCC between a template (projected sphere with the radius corresponding to that of a metal bead), and the projection data. By setting a threshold to define the NCC maxima, we could achieve an accurate metal bead center estimation from high noise levels datasets. Moreover, the optimization objective function relied only on the coordinate distances between synthesized projections calculated from 3D coordinates of the metal bead centers and extracted trajectories from projection data, hence to be robust to noise.

Furthermore, a small number of projections was needed to have a good estimation of the parameters. This was due to the robustness of investigating the projection trajectories of the metal bead centers as the optimization criteria as theoretically, to define each trajectory required knowing only five individual projected points. However, in our experiments, we observed that the errors started soaring after reducing number of projections to below ten. This could be attributed to numerical errors occurred during the preprocessing operations to extract the metal bead centers, so that more projections were needed to define the "correct" trajectories.

The simulation experiments demonstrated the feasibility to use our proposed LEGO phantom to calibrate various X-ray systems. Moreover, a small number of projections was needed to have accurate calibration results, which will take less time to acquire when calibrating a practical system. LEGO bricks are used to build the supporting structure, hence we have high flexibility to design its shape and size to adapt to the target system. There is only a minor limitation in that the supporting structure size depends on the size of the LEGO bricks. Therefore when the size of the system is smaller than the smallest LEGO brick, we cannot construct a suitable LEGO calibration phantom.

In future work, we will exploit the LEGO calibration phantom to reconstruct the objects acquired from the $3D^2$YMOX system which is our main goal for designing the LEGO phantom. We will start the reconstruction experiment with the calibration

phantom itself to make the comparison before and after calibrating the geometry parameters.

5 Conclusion

A LEGO calibration phantom is a low-cost and reliable solution for calibrating the geometry of an X-ray system. In this paper, we presented a simple but effective method to construct and use a LEGO phantom to calibrate the $3D^2YMOX$ system. The results on the simulation datasets with different noise levels and number of projections as well as varied number of the metal beads demonstrated the feasibility, flexibility, and robustness of our proposed method to calibrate an X-ray system. The experimental results on two different LEGO phantoms showed that our proposed method can be applied to different X-ray systems.

Acknowledgements

This work has been supported by the University Research Fund, UAntwerp BOF-GOA 2016 33927 and the Research Foundation - Flanders (FWO) SBO project MetroFlex (S004217N).

References

[1] 3D2YMOX (2018-06-19). https://www.uantwerpen.be/en/research-groups/3d2ymox/.

[2] Azevedo, S. G., Schneberk, D. J., Fitch, J. P., and Martz, H. E. (1990). Calculation of the Rotational Centers in Computed Tomography Sinograms. *IEEE Transactions on Nuclear Science*, **37**(4), 1525–1540.

[3] Chetley Ford, J., Zheng, D., and Williamson, J. F. (2011). Estimation of CT cone-beam geometry using a novel method insensitive to phantom fabrication inaccuracy: Implications for isocenter localization accuracy. *Medical Physics*, **38**(6Part1), 2829–2840.

[4] Cho, Y., Moseley, D. J., Siewerdsen, J. H., and Jaffray, D. a. (2005). Accurate technique for complete geometric calibration of cone-beam computed tomography systems. *Medical physics*, **32**(4), 968–983.

[5] Gullberg, G. T., Tsui, B. M., Crawford, C. R., Ballard, J. G., and Hagius, J. T. (1990). Estimation of geometrical parameters and collimator evaluation for cone beam tomography. *Medical Physics*, **17**, 264–272.

[6] Kingston, A., Sakellariou, A., Varslot, T., Myers, G., and Sheppard, A. (2011). Reliable automatic alignment of tomographic projection data by passive auto-focus. *Medical physics*, **38**(9), 4934–45.

[7] Levine, Z. and Grantham, S. (2008). A low-cost fiducial reference phantom for computed tomography. *Journal of Research of the National Institute of Standards and Technology*, **113**(6), 335–340.

[8] Lewis, J. P. (2001). Fast Normalized Cross-Correlation. *British Journal of Ophthalmology*, **67**(5), 315–316.

[9] Liu, Y. (2001). Improve industrial cone-beam computed tomography by integrating prior information. *ETH Zürich: Research Collection*, pages 12–19.

[10] Marinovszki, Á., De Beenhouwer, J., and Sijbers, J. (2018). An efficient CAD projector for X-ray projection based 3D inspection with the ASTRA Toolbox. *8th Conference on Industrial Computed Tomography*, pages 1–6.

[11] Noo et al., F., Clackdoyle, R., Mennessier, C., White, T. A., and Roney, T. J. (2000). Analytic method based on identification of ellipse parameters for scanner calibration in cone- beam tomography. *Physics in Medicine and Biology*, **45**, 3489–3508.

[12] Parkinson, D. Y., Knoechelb, C., Yang, C., Larabellb, C. A., and Le Gros, M. A. (2012). Automatic alignment and reconstruction of images for soft x-ray tomography. *Journal of Structural Biology*, **76**, 211–220.

[13] Quercioli, F., Tiribilli, B., Mannoni, A., and Acciai, S. (1998). Optomechanics with LEGO. *Applied Optics*, **37**(16), 3408.

[14] van Aarle, W., Palenstijn, W. J., Cant, J., Janssens, E., Bleichrodt, F., Dabravolski, A., De Beenhouwer, J., Batenburg, K. J., and Sijbers, J. (2016). Fast and flexible x-ray tomography using the astra toolbox. *Optics Express*, **24**(22), 25129–25147.